

## TURBULENCE CHARACTERIZATION OF A NON-REACTING FLOW ON A DELFT BURNER

**Luiz E. M. Lima, luizeduardomlima@yahoo.com.br**

Instituto Nacional de Pesquisas Espaciais–INPE, Rod. Presidente Dutra, km 40, Cachoeira Paulista - SP - Brasil, CEP 12630-000.

**Márcio T. Mendonça, marcio@iae.cta.br**

Comando Geral de Tecnologia Aeroespacial, Instituto de Aeronáutica e Espaço–CTA/IAE, Pç. Mal. Eduardo Gomes, 50, São José dos Campos - SP - Brasil, CEP 12228-904.

**Abstract.** *Coaxial round jets issuing from nozzles are typical configurations for applications such as diffusion flame burners. The turbulent characteristics of the flow are relevant for the burner efficiency and have a significant effect on pollutant emission due to improper mixing of fuel and oxidizer or inadequate residence times. In this work the main turbulent characteristics of coaxial jets out of a Delft burner configuration is investigated numerically. Simple coaxial jet results are available in the literature showing that the jet topology can be divided in two main regions, a developing region and a self-similar region. This topology is considerably changed for the Delft burner configuration where a large recirculation zone is found. For the Delft burner the jet spreading rate and the decay of the centerline velocity, along with streamwise and radial mean velocity profiles are presented for the regions near the nozzle exit and the region farther downstream. The spatial distribution of Reynolds stresses are also investigated. The investigation considers the effect of velocity ratio and velocity magnitude on the jet structure is investigated as well as the turbulent intensity at the nozzle exit. Particular attention is given to the large recirculation zone on the pilot flame holder zone and the effect of the governing parameters on the total length and turbulent characteristics of this region, which has a large impact on the flow downstream. The numerical approach is based on a control volume, incompressible RANS formulation with  $k - \epsilon$  turbulence model. Different versions of the turbulence model are considered, including RNG and non-linear models. The code used for the investigation is the Open Source FOAM CFD toolbox, which was used as a test bench for the proposed investigation without any modifications.*

**Keywords:** *Delft burner, turbulent coaxial jets, turbulent flow.*

### 1. INTRODUCTION

Jet flows are important canonical flows with many practical engineering applications such as in combustion and propulsion. They have been studied extensively theoretically, experimentally and numerically throughout the years. In turbofan exhaust the external cold air flow guarantees the reduction of intense noise levels from the central jet of higher speed, turbulence levels and temperature. Another important application is found in burners of diffusion flames, where the fuel flow of the central jet is surrounded by an external air jet that supplies the oxidant. In both cases the structure of the turbulent flow determines the source of jet noise and the diffusion of momentum and species (oxidant and fuel). Therefore, controlling the jet parameters can lead to a noise reduction or to a more efficient combustion (Verzicco and Orlandi, 1994). This control requires a detailed knowledge of the turbulence statistics, that is, the Reynolds stresses.

Champagne and Wygnanski (1971) (CW) investigated turbulent coaxial jets experimentally using hot wire anemometers. This experimental study was performed varying the area ratio ( $A_o/A_i$ ) and the velocity ratio ( $U_o/U_i$ ) between the internal and external jets in order to get the profiles of mean velocities, turbulent intensities and shear stresses. The flow was considered as being composed of two regions as shown in Fig. 1(a). The first region, a flow development region, formed by the internal and external potential cores, the mixing layers between the two jets and the mixing layer between the external jet and the environment. The second, a similarity region (or developed region), where the flow is completely developed and self-similar. In the similarity region the jet becomes identical to the axisymmetric simple jet. The thickness of each potential core decreases approximately linearly with longitudinal distance from the nozzle exit and the core region ends when the annular mixing regions are joined.

The behavior of turbulent coaxial jets was also studied experimentally by Buresti et al. (1998), for two velocity ratio,  $U_i/U_o = 0.30$  and  $0.67$ , keeping constant the diameter ratio,  $D_i/D_o = 0.5$ . As expected, they observed a reduction in the length of the internal potential core with the reduction of the velocity ratio, and for  $U_i/U_o = 0.30$ , the length became comparable to the external potential core. This condition results in larger fluctuations and a stronger level of mixing between the two flows. The evolution of the flow and the mixing between the internal and external jets are controlled by the direction, force, mutual position and consequent dynamics of the vortical structures that are presented in the development of the shear layers between the two jets and between the external jet and the fluid environment.

Rehab et al. (1997) conducted experimental studies on different flow regimes for coaxial jets of large velocity ratio  $1 < r_u \leq \infty$ . Two flow regimes can be identified if the velocity ratio ( $r_u \equiv U_o/U_i$ ) is large or smaller than the value of the critical velocity ratio  $r_{uc}$ . The value of  $r_{uc}$  range from 5 to 8, depending on the velocities profile in the nozzle

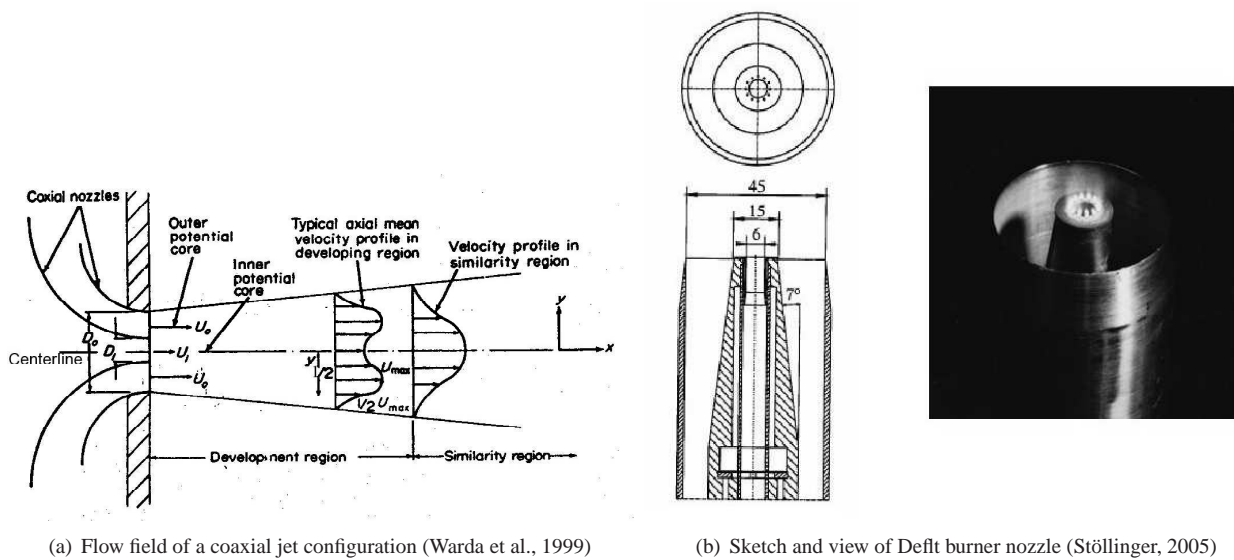


Figure 1. Examples of coaxial jet configurations.

exit. When  $r_u < r_{uc}$ , the fast annular jet periodically compresses the slower central jet near the internal potential core. The compression frequency corresponds to the frequency of oscillation of the external jet. When  $r_u > r_{uc}$ , the internal potential core is truncated and followed by a bubble of non-stationary recirculation with low oscillation frequency. The transition of one regime to another can be explained by a simple model whose ingredients are the entrainment, that it is governed by the mixing layer of the external jet, and mass conservation.

Warda et al. (1999) had experimentally investigated the influence of the variation in the velocity ratio in the flow of coaxial jets. These experimental inquiries on coaxial jets had shown that the radial distribution of the axial mean velocities and the turbulent intensities of the central and annular jets can be divided in three different regions, forming the topology of the jet flow. The initial region is located between the nozzle and the end of the external potential core. Immediately after, is the intermediate region which finishes in the reattachment point, and finally the region of complete mixing is established. The internal potential core is extremely dependent of the velocity ratio and the external potential core is little dependent of the velocity ratio for  $U_i/U_o > 1$ . It was observed that the increase in the velocity in the exit of the jet results in a reduction of the growth rate of the jet. Still it was observed that after the reattachment point coaxial jet thickness grows like a simple jet. Moreover, the similarity of the radial profiles of axial mean velocities was observed in the region of complete mixing. They had also studied the effect of the magnitude of the initial axial mean velocities of the coaxial jet for a fixed velocity ratio. regarding this effect, their results show that the reduction in the absolute value of the velocities of the internal and external flows, keeping constant the velocity ratio, makes the jet decay faster throughout the centerline.

In the present study, some configurations of turbulent coaxial jets had been analyzed. The results for a configuration of coaxial jets with  $U_o/U_i = 5$  and  $A_o/A_i = 2.94$ , are compared with the experimental results of Champagne and Wagnanski (1971), with the same configuration. The analysis of this configuration is used to validate the numerical procedure. Another simulation of an isothermal flow of coaxial jets was carried, with an area ratio identical to the Delft burner nozzle (Fig. 1(b)).

The objective of analyzing these configuration is to understand the turbulent characteristics of this type of burner, to verify the influence of the area ratio of the nozzle and to observe the influence of the presence of the thick wall between the internal and external ducts. These analysis play an important role in better understanding the flow dynamics in this type of device.

## 2. GOVERNING EQUATIONS AND NUMERICAL MODEL

The present numerical study of turbulent coaxial jets was done using a open source library in  $C++$ , for Computational Fluid Dynamics, called OpenFOAM. The numerical model if bases on the solution of the averaged Navier-Stokes equations (RANS) for incompressible flows using a finite volume method on structured non-uniform grid. The turbulent stress terms were closed with a two equations  $k - \epsilon$  turbulence model, that will be presented below.

## 2.1 Reynolds Averaged Navier-Stokes (RANS) Equations

The RANS equations are time averaged Navier-Stokes equations written for the instantaneous velocity decomposed in a mean value and a fluctuation. For an incompressible Newtonian fluid, these equations can be written as:

$$\frac{\partial \bar{u}_i}{\partial x_i} = 0, \quad (1)$$

$$\frac{\partial \bar{u}_i}{\partial t} + \frac{\partial}{\partial x_j} (\bar{u}_j \bar{u}_i) = \bar{f}_i + \frac{\partial}{\partial x_j} \left[ -\frac{\bar{p}}{\rho} \delta_{ij} + \nu \left( \frac{\partial \bar{u}_i}{\partial x_j} + \frac{\partial \bar{u}_j}{\partial x_i} \right) - \overline{u'_i u'_j} \right], \quad (2)$$

where  $u$  is the velocity,  $x$  is the space coordinate,  $t$  is the time,  $f_i$  is the volume force,  $p$  is the pressure,  $\rho$  is the specific mass,  $\delta_{ij}$  is the delta of Kronecker and  $\nu$  is the kinematic viscosity.

The left side of Eq. 2 represents the time variation of momentum due to the transient regime and the convection in the mean flow. The transient term is kept for numerical integration purposes. This variation is balanced by the mean volume force, the average pressure gradient, the viscous stresses and the apparent viscous stresses ( $-\overline{u'_i u'_j}$ ) due to fluctuations in the velocities field, generally known as the Reynolds stresses.

## 2.2 Turbulence Models

The turbulence models used for the simulation of the cases of coaxial jets in this work are: the  $k - \epsilon$  standard model; the  $k - \epsilon$  RNG model and the  $k - \epsilon$  Non-linear model of Shih. As the  $k - \epsilon$  Non-linear model of Shih present better results when compared to the experimental results available in the literature this model was used in all subsequent coaxial jet cases. The non-linear model is designed to give an improved performance through the inclusion of quadratic components of stresses and vorticity to capture anisotropies. The common factor between all non-linear cubical models is a general constituent equation that relates the Reynolds stresses tensor to all the quadratic and cubical combinations of the strain rate tensor and the vorticity. Using the turbulent kinetic energy and its rate of the dissipation to represent the velocity and the turbulent length scales, this equation can be written of the following form (Chen et al., 1998).

$$\begin{aligned} \frac{\overline{u'_i u'_j}}{k} &= \frac{2}{3} \delta_{ij} - 2 \frac{\nu_t}{k} \overline{S_{ij}} + c_1 \frac{\nu_t}{\hat{\epsilon}} \left( \overline{S_{ik}} \overline{S_{kj}} - \frac{1}{3} \delta_{ij} \overline{S_{kl}} \overline{S_{kl}} \right) \\ &+ c_2 \frac{\nu_t}{\hat{\epsilon}} \left( \overline{\Omega_{ik}} \overline{S_{kj}} + \overline{\Omega_{jk}} \overline{S_{ki}} \right) + c_3 \frac{\nu_t}{\hat{\epsilon}} \left( \overline{\Omega_{ik}} \overline{\Omega_{jk}} - \frac{1}{3} \delta_{ij} \overline{\Omega_{kl}} \overline{\Omega_{kl}} \right) \\ &+ c_4 \frac{\nu_t k}{\hat{\epsilon}^2} \left( \overline{S_{ki}} \overline{\Omega_{lj}} + \overline{S_{kj}} \overline{\Omega_{li}} \right) \overline{S_{kl}} + c_5 \frac{\nu_t k}{\hat{\epsilon}^2} \left( \overline{S_{kl}} \overline{S_{kl}} - \overline{\Omega_{kl}} \overline{\Omega_{kl}} \right) \overline{S_{ij}}. \end{aligned} \quad (3)$$

Where  $\overline{S_{ij}}$  is the average component of the strain rate tensor given by:

$$\overline{S_{ij}} = \frac{1}{2} \left( \frac{\partial \bar{u}_i}{\partial x_j} + \frac{\partial \bar{u}_j}{\partial x_i} \right), \quad (4)$$

and  $\overline{\Omega_{ij}}$  is the average component of the vorticity tensor given by:

$$\overline{\Omega_{ij}} = \frac{1}{2} \left( \frac{\partial \bar{u}_i}{\partial x_j} - \frac{\partial \bar{u}_j}{\partial x_i} \right). \quad (5)$$

Different variations of the model appear due to different approaches in the determination of the coefficients  $c_1$  to  $c_5$  and the differences in the determination of the scales in the transport equations.

The turbulent kinetic energy  $k$ , the turbulent viscosity  $\nu_t$  and the homogeneous dissipation rate  $\hat{\epsilon}$ ,

$$\hat{\epsilon} = \epsilon - 2\nu \left( \frac{\partial \sqrt{k}}{\partial x_i} \right)^2, \quad (6)$$

they are obtained, respectively, for:

$$\nu_t = C_\mu f_\mu \frac{k^2}{\hat{\epsilon}}, \quad (7)$$

$$\frac{\partial}{\partial x_i} (\bar{u}_i k) = \frac{\partial}{\partial x_j} \left[ (\nu + \nu_t) \frac{\partial k}{\partial x_j} \right] + P_k - \epsilon, \quad (8)$$

$$\frac{\partial}{\partial x_i}(\overline{u_i \hat{\epsilon}}) = \frac{\partial}{\partial x_j} \left[ \left( \nu + \frac{\nu_t}{1,3} \right) \frac{\partial \hat{\epsilon}}{\partial x_j} \right] + \frac{\hat{\epsilon}}{k} (C_{1\epsilon} P_k - C_{2\epsilon} \hat{\epsilon}) + E_{\hat{\epsilon}} + Y, \quad (9)$$

where  $P_k$  is the term of production of kinetic energy,  $f_{\mu}$  is the damping coefficient,  $Y$  is the Yap correction, and  $C_{\mu}$ ,  $C_{1\epsilon}$  and  $C_{2\epsilon}$  are model constants.

### 3. RESULTS

The results for the cases of coaxial jets analyzed in this work are presented here. The detailed configuration of the cases of coaxial jets analyzed in this work is described in Tab. 1.

Table 1. Configuration of the coaxial jets analyzed.

Case	$U_o/U_i$	$U_i$ ( $ms^{-1}$ )	$U_o$ ( $ms^{-1}$ )	$A_o/A_i$	$D_i \times 10^3$ ( $m$ )	$D_o \times 10^3$ ( $m$ )	$D_W \times 10^3$ ( $m$ )
1	5	12	60	2,94	25,4	50,41756	–
2	0,2	60	12	2,94	25,4	50,41756	–
3	0,202	21,8	4,4	28,13	8	42,43	–
4	0,202	21,8	4,4	28,13	8	45	15

Comments:  $D_W$  it is the thickness of the wall between the internal and external jets.

Where  $U$  is the exit velocity,  $A$  is the nozzle area,  $D$  is the nozzle diameter, the subscripts  $o$  and  $i$  represent the outer and inner jets.

The initial and boundary conditions in the interior and at the boundaries of the computational domain must be specified for each case. They are given by the turbulent kinetic energy distribution, dissipation rate of turbulent kinetic energy, speeds, pressures and etc., moreover kinematic viscosity must be specified. Due the presence of the edge between the internal and external jets in case 4, wall functions had been specified in the boundary conditions of the corresponding edge faces. A description of the boundary conditions for each case is given in Tab. 2.

Table 2. Boundary Conditions.

Case	$Re_{D_i} \times 10^{-5}$	$Re_{D_o} \times 10^{-5}$	$I(\%)$	$L/D_o$	$k(m^2s^{-2})$	$\epsilon(m^2s^{-3})$
1	0,2	0,96	5	0,05	13,5	3233,2
2	1	0,4	5	0,05	0,54	25,87
3	0,087	0,093	5	0,05	0,0726	1,5151
4	0,087	0,099	5	0,05	0,0726	1,4286

Where  $Re$  is the Reynolds number,  $I$  is the turbulent intensity and  $L$  is scale of turbulent length.

#### 3.1 Coaxial Jets (Case 1)

This case was used to validate the numerical procedure by comparison of results with the experimental work of Champagne and Wygnanski (1971). The coaxial jet have an area ratio  $A_o/A_i = 2.94$  and velocity ratio  $U_o/U_i = 5$  as described in Tab. 1.

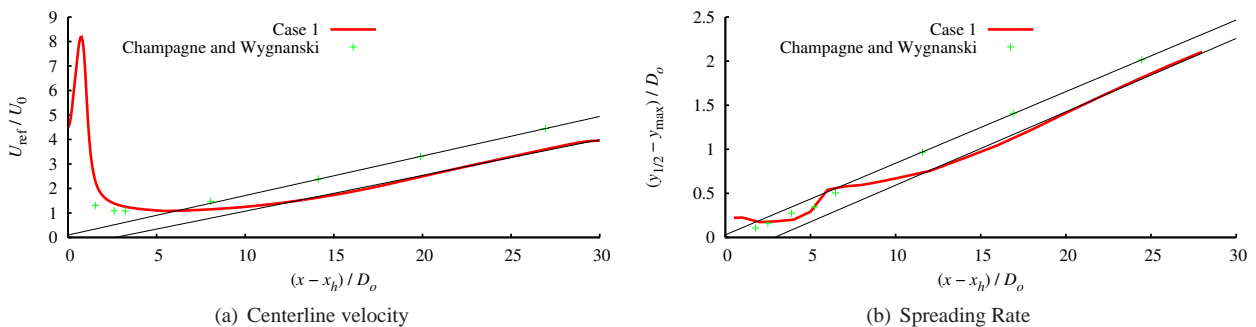


Figure 2. Variation of centerline velocity  $U_0$  and growth of jet's half-width  $y_{1/2}$  for  $U_o/U_i = 5$  and  $A_o/A_i = 2.94$ .

In Figure 2, it is possible to observe that the centerline velocity  $U_0$  and jet's half-width  $y_{1/2}$  vary linearly from  $x/D_o > 14$  and  $x/D_o > 10$ , respectively, corresponding to the developed similar region. The results from Champagne and Wygnanski (1971) show that the centerline velocity and jet's half-width varies linearly from  $x/D_o > 11$  and  $x/D_o > 8$ , respectively. The numerically obtained spreading rate ( $S = 0.083$ ) is very close to the experimental value ( $S = 0.081$ ).

The observed differences are related to the limitations of the turbulence model, and with the quality of the computational mesh due to hardware limitations. It is important to observe that despite these differences, the numerical results present a strong correlation with the experimental results.

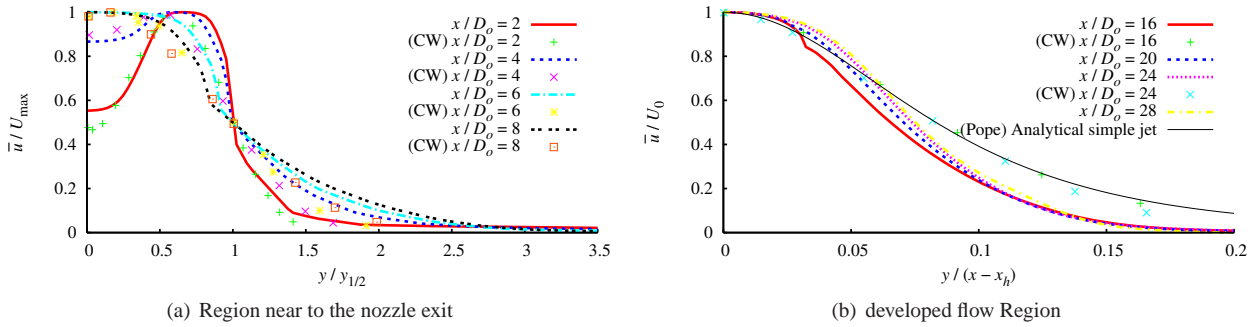


Figure 3. Normalized velocities profile for  $U_o/U_i = 5$  and  $A_o/A_i = 2.94$ .

The profiles of mean velocities can be observed in Fig. 3. In the region near to the nozzle exit (Fig. 3(a)), the profiles of mean velocities present good quantitative agreement with the experimental results, and the curves have the same characteristic form of the experimental results of Champagne and Wygnanski (1971). In the region of developed flow (Fig. 3(b)), the self-similar profiles also present good agreement with experimental results and the analytical profile for simple jet.

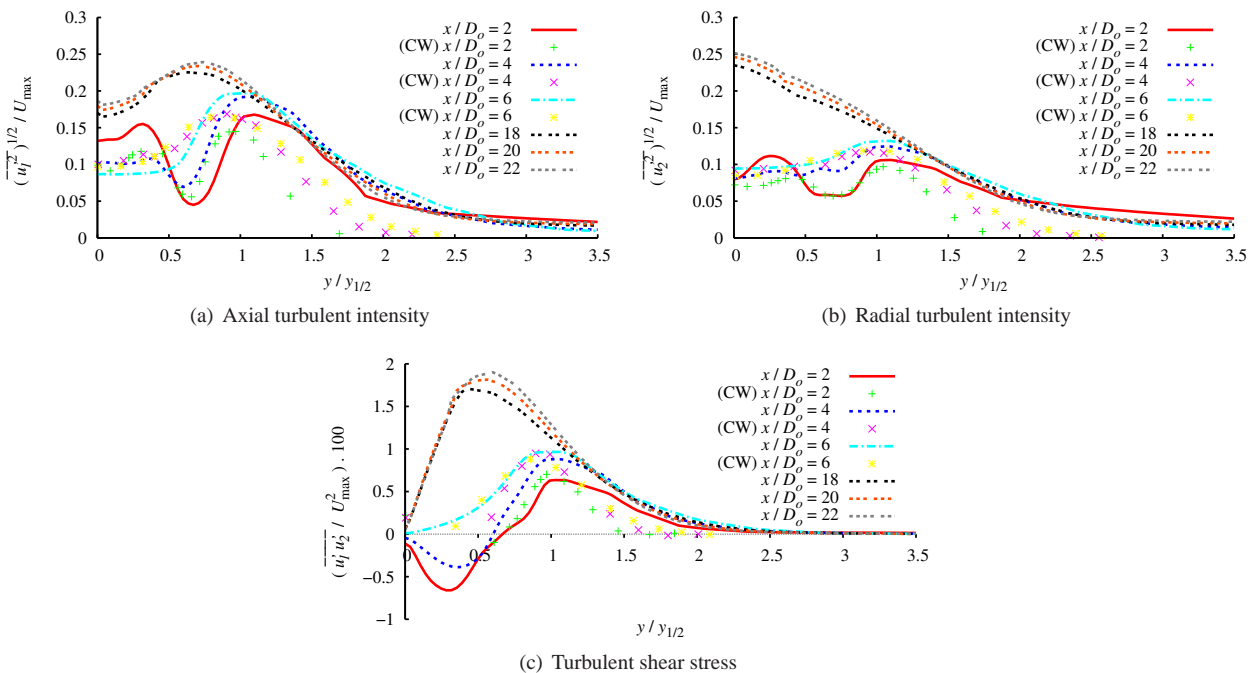


Figure 4. Reynolds stresses distributions for  $U_o/U_i = 5$  and  $A_o/A_i = 2.94$ .

In Figure 4, it is possible to observe the distributions of the Reynolds stresses for the case analyzed in comparison with experimental results. Up to a longitudinal distance  $x/D_o < 6$  is possible to observe the presence of two peaks characterizing the internal and external mixing layers. Beyond this point there is only the internal potential core, and consequently, a mixing layer between the jet and the ambient. The Reynolds stresses tend to an auto-similar behavior. The similarity region was found for  $x/D_o > 18$ . In this region the profiles of each component of the Reynolds stresses have the same characteristic form and the values are very close, almost coinciding in one single curve.

The profiles of the turbulent properties can be seen in Fig. 5. up to  $x/D_o < 6$ , is also possible to observe the presence of two peaks in the profiles of the turbulent properties. These peaks correspond to the presence of the internal and external mixing layers. beyond this point, it is only possible to observe the presence of only one peak, corresponding to the external

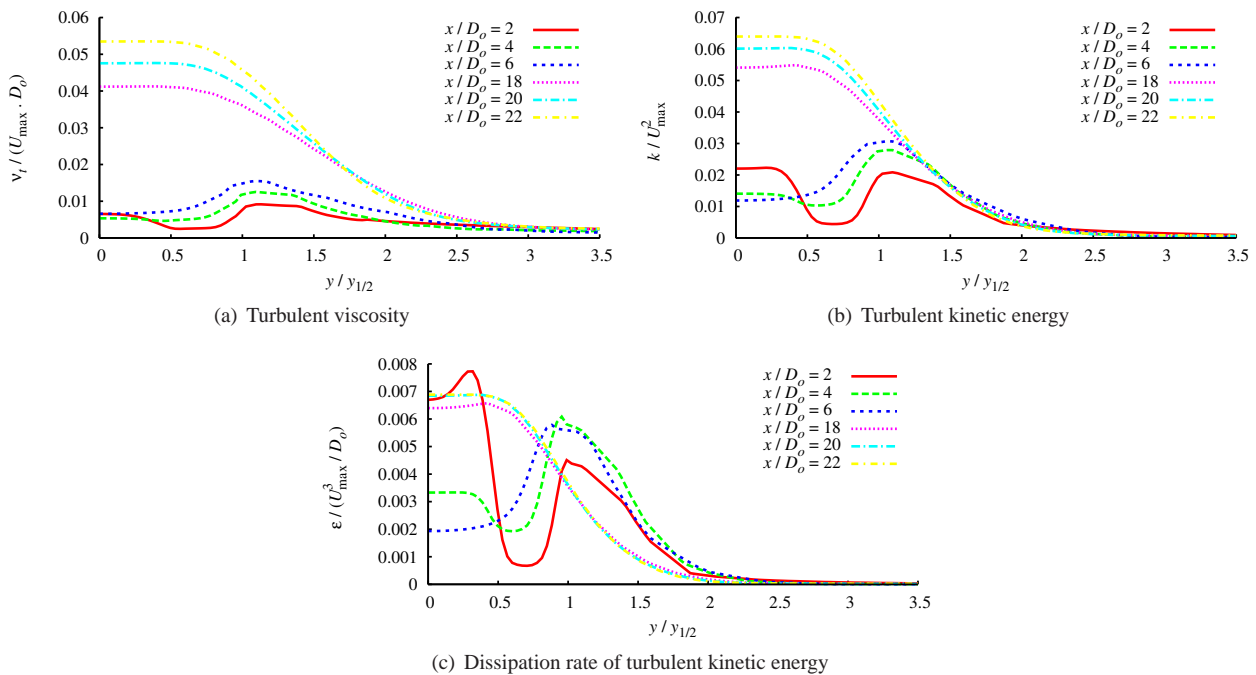


Figure 5. Turbulent properties distributions for  $U_o/U_i = 5$  and  $A_o/A_i = 2.94$ .

mixing layer. From  $x/D_o > 18$ , as the peak disappear characterizing the complete disappearance of the layer of external mixing. The presence of these peaks, that characterize the presence of the potential core and the mixing layers, also can be observed for the Reynolds stresses (Fig. 4). For the turbulent shear stress (Fig. 4(c)) these peaks are characterized by a point of minimum (internal potential core) and a point of maximum (external potential core) as observed experimentally. Despite the observed differences, the numerical model is able to capture the physical behavior of the flow of coaxial jets.

### 3.2 Burner with Thin Wall Between the Nozzles (Cases 2 and 3)

Case 3 consists of a coaxial jets with a configuration of a Delft burner, disregarding the presence of the thick wall between the internal and external jets. Case 2 was compared to case 3 to show the influence of the increase in the area ratio in the flow. In the two cases the velocity ratio is the same one.

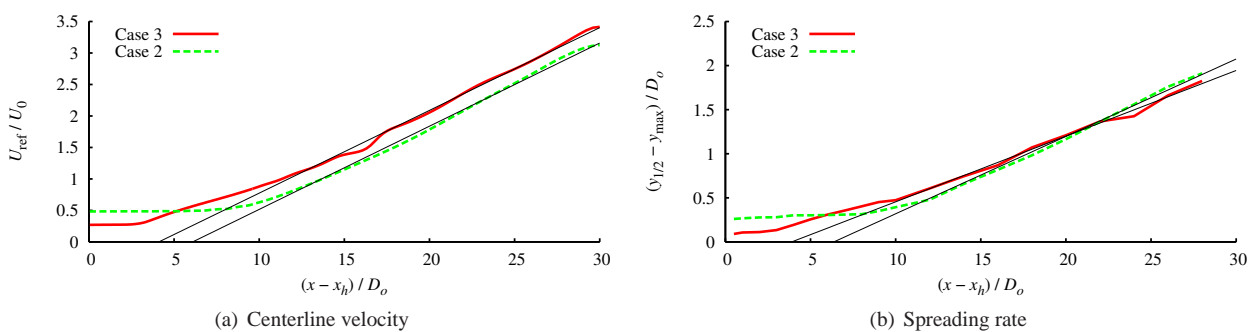


Figure 6. Variation of centerline velocity  $U_0$  and growth of jet's half-width  $y_{1/2}$  for  $U_o/U_i = 0.202$  and  $A_o/A_i = 28.13$ .

In Figure 6 is possible to observe the variation of centerline velocity and the growth of jet's half-width. The oscillations observed in the centerline velocity can be related to recirculation zones in the flow, which had the largest area ratio between the two ducts. The spreading rate for this case ( $S = 0.075$ ) presents a lower value in comparison with case 2 ( $S = 0.087$ ). The larger area ratio provides a reduction in the entrainment between the external jet and surrounding fluid. That is, a lower amount of surrounding fluid is dragged by the jet, having diminished the half-width and therefore a lower spreading rate results. Entrainment is the process in which fluid from the surroundings is drawn into the turbulent zone and is the main cause of the spreading of turbulent flows (including wall boundary layers) in the flow direction (Versteeg and Malalasekera, 1995). Initially fast moving jet fluid will lose momentum to speed up the stationary surrounding fluid. Owing to the entrainment of the surrounding fluid the velocity gradients decrease in magnitude in the flow direction. This causes the decrease of the mean velocity of the jet in the centerline.

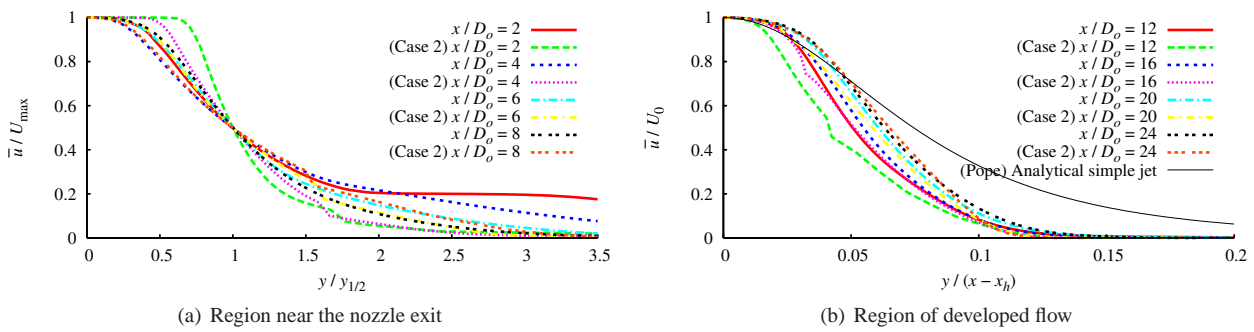


Figure 7. Normalized velocities profiles for  $U_o/U_i = 0.202$  and  $A_o/A_i = 28.13$ .

In Figure 7, the mean velocities profiles are presented in the region near to the nozzle exit (Fig. 7(a)) and in the developed flow region (Fig. 7(b)). It is possible to observe that the velocities profiles for this case tend a similar form from  $x/D_o = 20$ .

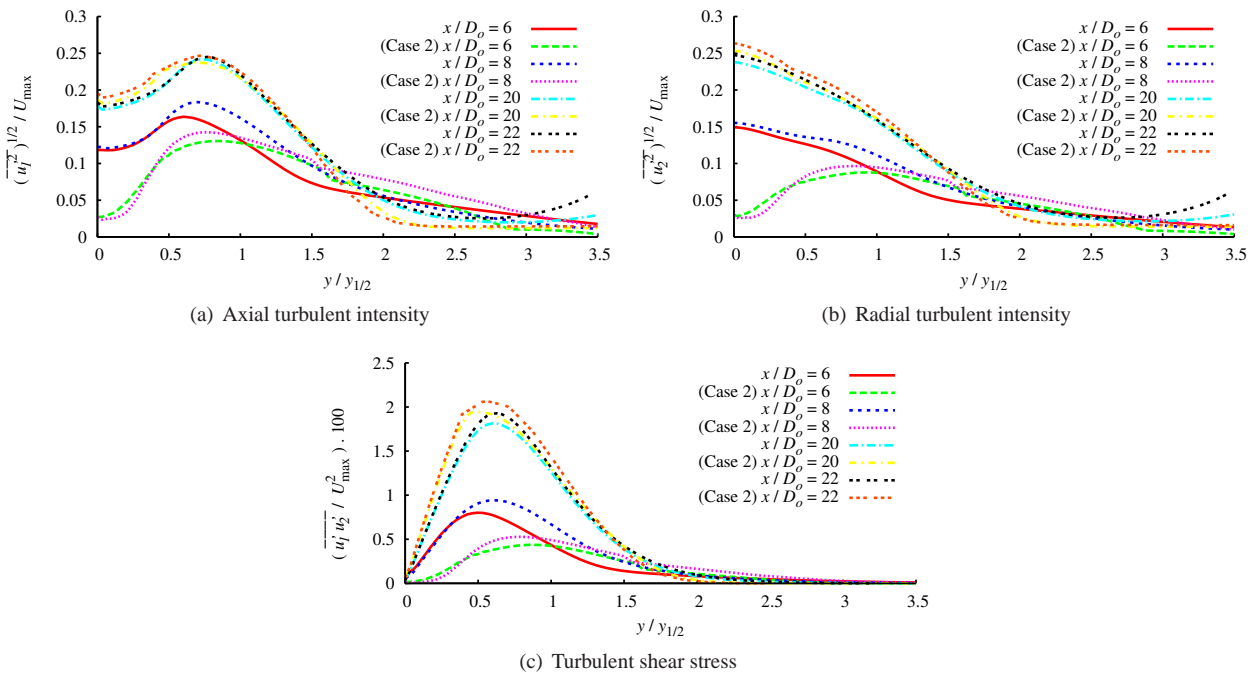


Figure 8. Reynolds stresses distributions for  $U_o/U_i = 0.202$  and  $A_o/A_i = 28.13$ .

It is possible to observe, that the larger area ratio results in an increase in the Reynolds stresses in the region near to the nozzle ( $x/D_o = 8$ ), as seen in Fig. 8. In the developed flow region, is possible to see that in  $x/D_o = 20$ , the Reynolds stresses for case 3 present larger values than case 2. Next to the nozzle, the peak of the stress is dislocated inward. The radial turbulent intensity has maximum in the center in the region near to the nozzle for case 3, whereas in case 2 the maximum is located in  $y/y_{1/2} = 1$  at least until  $x/D_o = 8$ . This may result in stronger mixing between the internal and external jets for case 3.

The similarity region starts in  $x/D_o > 20$ . From this point the profiles of the Reynolds stresses present the same characteristic form and very close values for cases 2 and 3. It is possible to relate the improvement of the mixing between the flows of the two jets to the higher levels of turbulence in case 3, in the region near to the nozzle. In the region near to the nozzle, the profiles of the turbulent properties have a behavior similar to the behavior of the Reynolds stresses. This behavior can be observed in the Fig. 9. In the region near to the nozzle, it is possible to observe that in the turbulent properties for given case, the maximum occurs between  $0.5 < y/y_{1/2} < 1$ , whereas in case 2 the maximum if locates at  $y/y_{1/2} = 1$  at least until  $x/D_o = 8$ .

The disappearance of the internal potential core occurs from  $x/D_o > 20$ . From this point the maximum value of these properties remains constant in the region of the jet, and it does not have the presence of a characteristic maximum point.

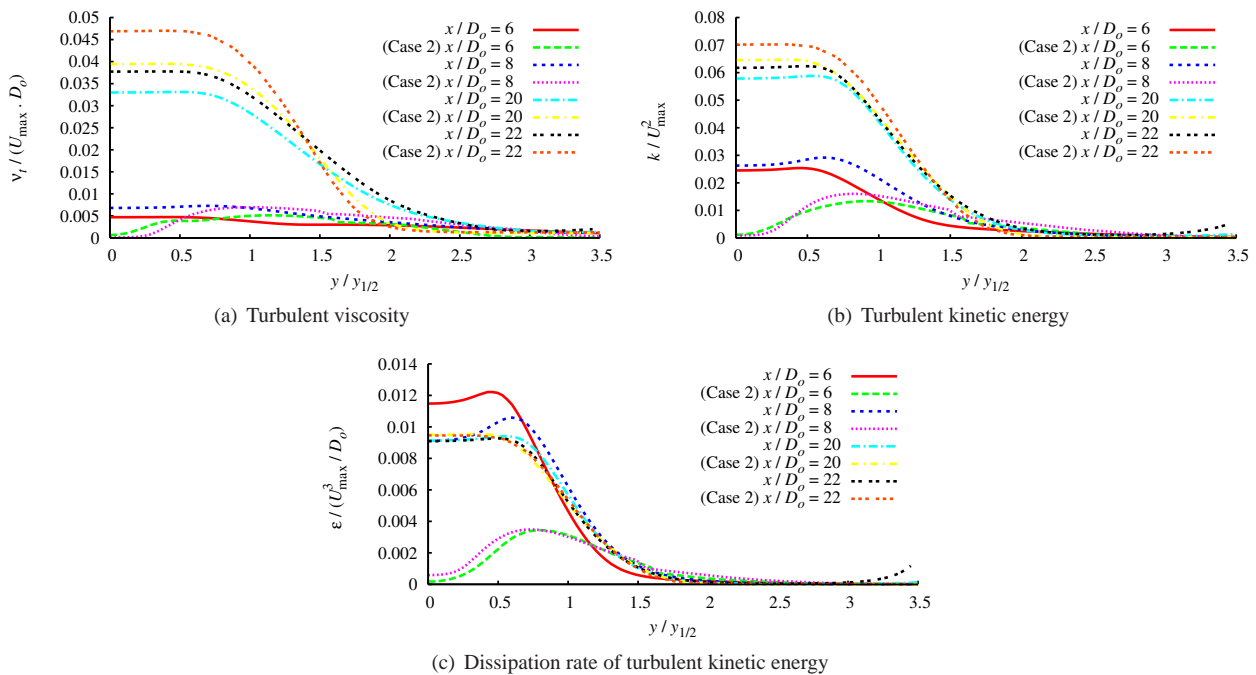


Figure 9. Turbulent properties distributions for  $U_o/U_i = 0.202$  and  $A_o/A_i = 28.13$ .

### 3.3 Burner with thick Wall between the Nozzles (Case 4)

This case consists of a coaxial jet with a configuration of diffusion flame Delft burner, considering the thick wall between the internal and external jets. This case is compared to case 3 to show the influence of the thick wall in the jet flow. Moreover, considering the presence of the edge between the internal and external jets, this configuration more adequately represents the Delft burner. However it must be considered that the pilot flames positioned on the thick wall are not considered in this runs.

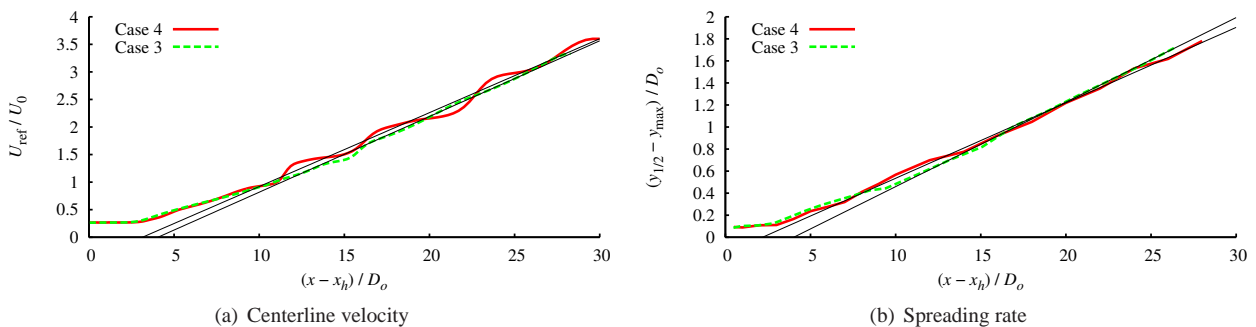


Figure 10. Variation of centerline velocity  $U_0$  and growth of jet's half-width  $y_{1/2}$  for  $U_o/U_i = 0.202$  and  $A_o/A_i = 28.13$  with wall between the internal and external jets.

In Figure 10, is possible to observe that the presence of the wall between the internal and external ducts increases the level of oscillations in the variation of the centerline velocity in the downstream direction. The spreading rate for this case ( $S = 0.068$ ) presents a lower value than that for case 3 ( $S = 0.075$ ). This means that the entrainment between external jet and surrounding fluid is lower for this case. The presence of the thick wall in the nozzle exit plan increases the intermittency of the flow, as observed by Abdel-Rahman et al. (1997). This phenomenon can be associated to the presence of zones of recirculation near the wall.

In Figure 11, is possible to visualize the velocities profiles. The velocities profiles have a faster convergence for an auto-similar profile than that for case 3 (Fig. 11(b)). This indicates a better mixing between the two jets. The distribution of the Reynolds stresses can be observed in Fig. 12. For the distance  $x/D_o > 6$ , the stresses present maximum values a little larger than that for case 3. From  $x/D_o > 22$ , the Reynolds stresses present a self-similar profile. For the case 3 this profile self-similar present from  $x/D_o > 20$ , where the internal potential core ends.

As observed in case 3, is possible to relate the improvement of the mixing between the flows of the two jets to the higher levels of turbulence, in the region near to the nozzle exit. But The Reynolds stresses distribution and maximum

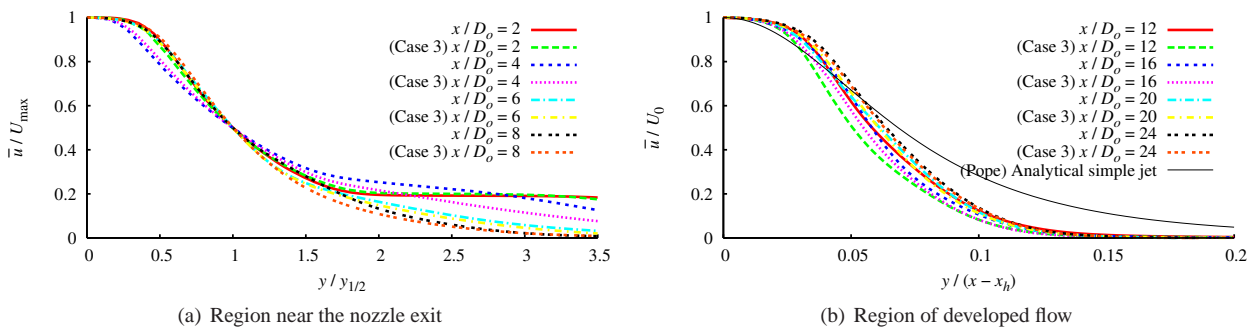


Figure 11. Normalized velocities profiles for  $U_o/U_i = 0.202$  and  $A_o/A_i = 28.13$  with wall between the internal and external jets.

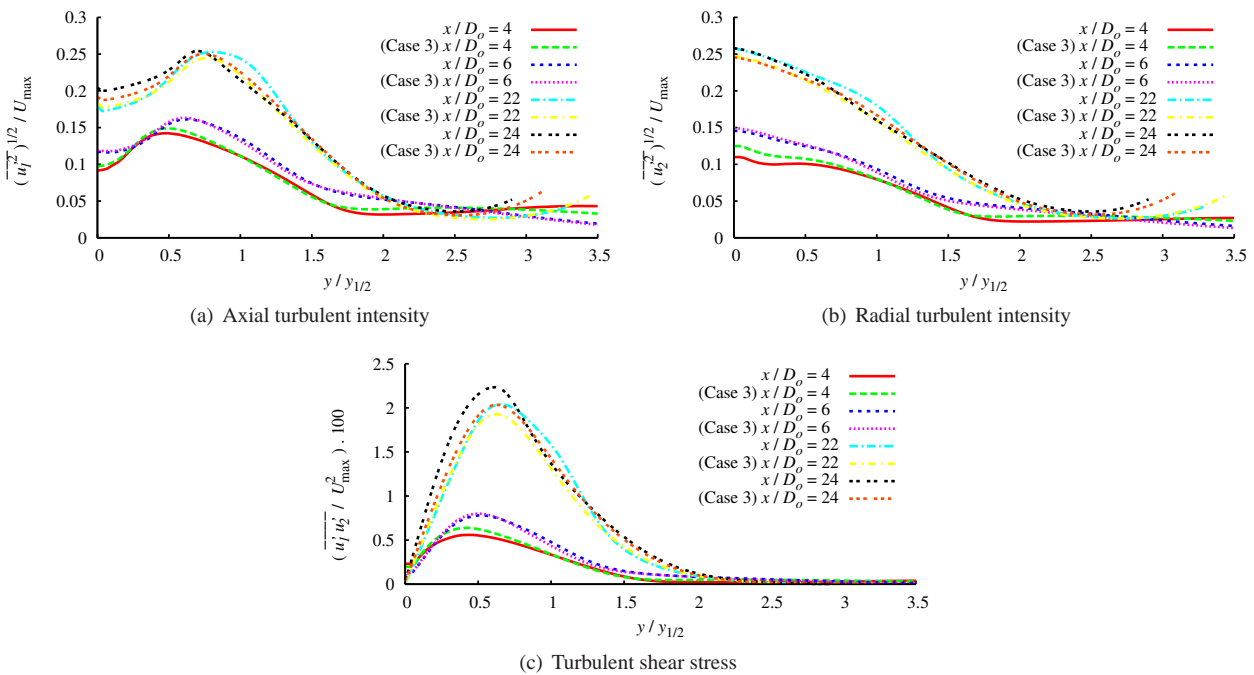


Figure 12. Reynolds stresses distributions for  $U_o/U_i = 0.202$  and  $A_o/A_i = 28.13$  with wall between the internal and external jets.

magnitude for cases 3 and 4 are very similar. Therefore, a more refined comparison of these profiles becomes difficult.

Figure 13 show the turbulent viscosity, the turbulent kinetic energy and the dissipation rate of turbulent kinetic energy for case 4 compared to case 3. The same behavior observed for the Reynolds stresses can also be observed for the turbulent properties. It is possible to observe that the internal potential core only disappears after  $x/D_o > 22$ , where the maximum value of the turbulent properties are constant in the jet region. In case 3, the internal potential core disappears after  $x/D_o > 20$ . The characteristic peaks in these properties, that represent the influence of the potential cores and the mixing layers, are similar with those of case 3.

#### 4. CONCLUSION

This work presented a numerical analysis of turbulent coaxial jets. The results were obtained with three different turbulent models:  $k - \epsilon$  standard,  $k - \epsilon$  RNG and  $k - \epsilon$  non-linear of Shih. The model that presented the best results for the coaxial jet topology was the non-linear  $k - \epsilon$  of Shih.

The first test case, used in the validation of the model, presented a good level of agreement with experimental results. The Cases 3 and 4, show that the increase of the area ratio provides increase in the Reynolds stresses, in the region near the nozzle, guarantees a good level of turbulence in this configuration. Due to these advantage in relation to the mixing process, the configuration of coaxial jets has been widely used in diffusion flame burners. This study allows a better understand for the behavior of turbulent coaxial jets.

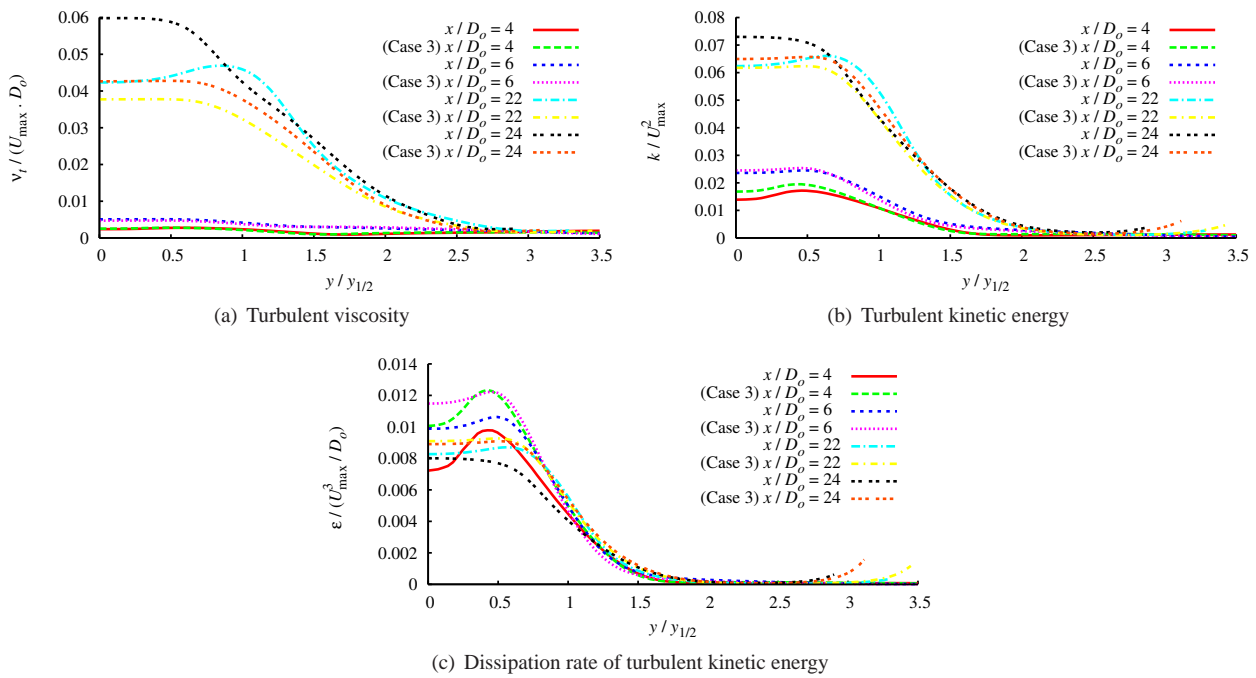


Figure 13. Turbulent properties distributions for  $U_o/U_i = 0.202$  and  $A_o/A_i = 28.13$  with wall between the internal and external jets.

## 5. REFERENCES

- Abdel-Rahman, A. A., Chakroun, W. and Al-Fahed, S. F., 1997, "LDA measurements in the turbulent round jet", *Mechanics Research Communications*, Vol. 24, No. 3, pp. 277–288.
- Buresti, G., Petagna, P. and Talamelli, A., 1998, "Experimental investigation on the turbulent near-field of coaxial jets", *Experimental Thermal and Fluid Science*, Vol. 17, pp. 18–36.
- Champagne, F. H. and Wynanski, I. J., 1971, "An experimental investigation of coaxial turbulent jets", *Int. J. Heat and Mass Transfer*, Vol. 14, pp. 1445–1464.
- Chen, W. L., Lien, F. S. and Leschziner, M. A., 1998, "Non-linear eddy-viscosity modelling of transitional boundary layers pertinent to turbomachine aerodynamics", *Int. J. of Heat and Fluid Flow*, Vol. 19, pp. 297–306.
- Rehab, H., Villermaux, E. and Hopfinger, E. J., 1997, "Flow regimes of large velocity ratio coaxial jets", *J. Fluid Mechanics*, Vol. 345, pp. 357–381.
- Versteeg, H. K. and Malalasekera, W., 1995, "An Introduction to Computational Fluid Dynamics - The Finite Volume Method", Longman Scientific & Technical.
- Verzicco, R. and Orlandi, P., 1994, "Direct simulations of the transitional regime of a circular jet", *Phys. Fluids*, Vol. 6, pp. 751.
- Warda, H. A., Kassab, S. Z., Elshorbagy, K. A. and Elsaadawy, E. A., 1999, "An experimental investigation of the near-field region of a free turbulent coaxial jet using LDA", *Flow Measurement and Instrumentation*, Vol. 10, pp. 15–26.
- Warda, H. A., Kassab, S. Z., Elshorbagy, K. A. and Elsaadawy, E. A., 2001, "Influence of the magnitude of the two initial velocities on the flow field of a coaxial turbulent jet", *Flow Measurement and Instrumentation*, Vol. 12, pp. 29–35.

## 6. Responsibility notice

The author(s) is (are) the only responsible for the printed material included in this paper